

# Assembly of Multi-Stranded Nanofiber Threads through AC Electrospinning

By Siddharth Maheshwari and Hsueh-Chia Chang\*

Electrospinning refers to the formation of micrometer and sub-micrometer fibers under the application of a strong electric field to a polymer fluid, solution, or melt.<sup>[1,2]</sup> Compared to other methods of fiber preparation like drawing, template synthesis, extrusion, phase-separation of polymeric mixtures, self-assembly of individual molecules, etc., electrospinning provides a robust method to form long fibers with a wide range of fiber diameters that can vary from nanometers to micrometers. Additionally, the basic setup for electrospinning is relatively uncomplicated and can be applied to a variety of polymer-solvent systems. These favorable attributes have led to the widespread study of electrospinning for applications in different fields including nanocomposites, biocatalysts, fabrics and protective clothing, optical sensing, drug delivery, wound dressing, tissue culture, filtration, etc.<sup>[3-9]</sup>

In synchrony with the study of electrospinning for many applications, there has also been significant fundamental interest in understanding the mechanism behind this process. Previous work on DC electrospinning/electrospinning has shown that under the application of an electric field, the meniscus deforms into a conical shape formed due to a balance between capillary and coulombic forces, and a liquid jet ejects out from the conical tip, which thins as it accelerates downstream.<sup>[10,11]</sup> After traversing a small distance in a straight-line path, the electrospun jet then undergoes a non-axisymmetric whipping instability that increases the effective jet path significantly and causes the jet to stretch and become extremely thin, leading to the formation of polymeric fibers with sub-micrometer dimension. This increase in path length due to whipping instability is responsible for the formation of ultrathin fibers with electrospinning. This instability is also behind the appearance of the characteristic conical whipping cloud that is just the trace of a single fiber jet oscillating very rapidly.<sup>[12]</sup> The whipping instability makes the accurate simulation of the jet path difficult, however, certain features like the operating regime for electrospinning as well as the appearance of the conical cloud have been predicted with accuracy.<sup>[13-15]</sup> The fibers formed via this technique predominantly form a mesh-like structure with a random orientation of fibers, hence there has been considerable effort directed toward

aligning fibers and controlling their orientation and placement.<sup>[16-18]</sup>

In contrast to the detailed study of DC electrospinning, there have been very few reports on electrospinning using an AC electric field; the few studies available have focused on either DC-superimposed AC fields,<sup>[19]</sup> or AC studies of electrospinning/electrospinning at a fixed frequency.<sup>[20,21]</sup>

Our preceding work on AC electrospinning had revealed a multitude of novel physical mechanisms, predominantly dependent upon the frequency time scale,<sup>[22,23]</sup> suggesting that AC electrospinning might be quite different from DC electrospinning. In this communication, we present our observations on the AC spinning phenomena and its dependence on the frequency time scale. We generate multi-stranded threads exhibiting a completely different morphology. Besides simplifying the characterization of nanofibers, this new fiber pattern and its strong frequency dependence can significantly extend the applicability of electrospinning for specific applications. We proceed by describing our observations, followed by an attempt to explain the mechanism behind this behavior.

The experimental setup consisted of a needle and a flat electrode connected to a high voltage AC system, a schematic is shown in Figure 1a. The fact that the spinning behavior under an AC field was different was obvious when a visible thread was seen emerging downstream from the needle instead of the mesh-like morphology seen with DC spinning. This thread could be more than a meter long and did not display any significant attraction toward the ground electrode, and consequently it could be easily deflected away. Once the thread descended below the ground electrode, it became totally free of any coulombic attraction from the electrode system, and could be easily deflected manually or even by weak air currents around the experimental setup. This eliminated the problems associated with fiber alignment and collection that is usually seen with DC spinning. This is experimentally demonstrated in Figure 1b, where a large thread could be manually woven onto a commercial coaxial cable. Mechanical spooling with a disk and rotor assembly should therefore be quite straightforward, suggesting that this technique can be easily scaled up for applications. Scanning electron microscopy (SEM) images, shown in Figure 2, revealed some very distinct features of these threads. They were actually a combination of multiple strands that were not only weaved or superimposed over each other, but were also, in fact, a continuous network with the strands fused together. The thread thickness was of the order of 10  $\mu\text{m}$  while the individual strands were approximately 100 nm thick, showing a large variation in size between them. Depending upon the applied potential and frequency, there could be 100 strands or more weaved to form a

[\*] Prof. H.-C. Chang, Dr. S. Maheshwari  
Chemical and Biomolecular Engineering Department  
Center for Microfluidics and Medical Diagnostics  
University of Notre Dame, Notre Dame, IN 46556 (USA)  
E-mail: hchang@nd.edu

DOI: 10.1002/adma.200800722

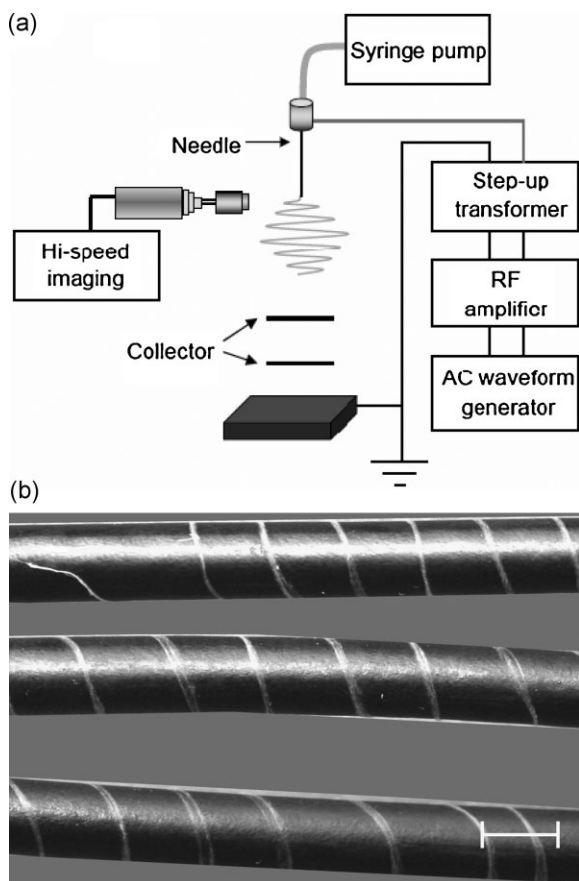


**Figure 1.** a) Schematic of the AC electrospinning experimental setup: the high voltage terminal from the step-up transformer is connected to the spinning needle, and the ground connection to a flat ground electrode. Collectors are placed between the needle and the ground electrode. b) Electrospun thread woven around a flexible cable, scale bar: 5 mm.

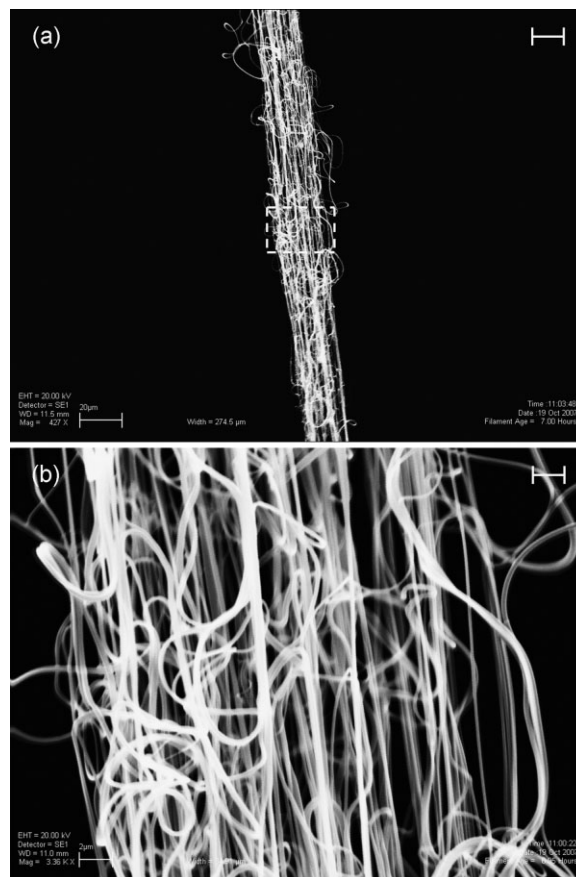


**Figure 2.** Thread morphology formed with AC electrospinning by applying a frequency of 50 Hz at a voltage of 3.3 kV<sub>RMS</sub> at a flow rate of 0.3 mL h<sup>-1</sup>. a) SEM image of the thread, scale bar: 20 μm. b) A blow-up of the dashed square in (a). The thread is seen to be composed of sub-micrometer fibers that are intricately bound together. The nanofibers are not just woven together but are actually connected, scale bar: 2 μm.

thread. Upon varying the applied potential and frequency, there was considerable variation in the appearance of the thread. The net width of the thread, the number of strands present, and bead formation on the strands were all very strongly dependent upon the operating conditions as shown in Figure 3. It was seen that increasing voltage increased the overall width and the number of strands in a thread, while suppressing bead formation. An increase in frequency had an exactly opposite effect. The contrary influences of the applied potential and frequency can be quantitatively confirmed from Figure 3e, where we have shown the effect of field conditions on the net width of the threads. Variation in net width with applied voltage is clearly linear while being inversely proportional to the applied frequency. Consequently it is possible to design threads with a desired morphology by varying the field conditions.

To understand these features of the fiber morphology, we proceeded to visualize the thread formation process by observing the vicinity of the needle in detail. We started by taking long exposure (20 ms) images of the spinning process with variation in the process conditions, since the long exposure provided a fully developed trace of the whipping cloud. A typical image is shown in

Figure 4a, which shows some characteristically different properties as compared to the DC electrospinning. Foremost among these is the shape of the whipping cloud, which is like the usual upright DC cone to begin with, but then changes into an inverted cone structure. The emergence of the fiber thread from the cusp of this cone was also visible. Additionally, unlike DC spinning there was no linear jet path emerging from the tip. It should also be noted that these characteristic features did not vary with the shape of the ground electrode. The effect of the operating field condition on the whipping cloud is shown in Figure 4b, where similar long exposure images at varying field conditions were taken and the sectional area of the whipping region was calculated. We again found that the influences of the applied potential and frequency were contrary to each other and the area of the whipping region increased with applied voltage while it decreased with applied frequency, displaying a linear and inverse trend, respectively.

A similar whipping envelope, with an upright cone followed by an inverted cone, had also been seen with DC electrospinning, when a very sharp ground electrode was used,<sup>[24]</sup> which can be explained by the localization and enhancement of the electric field at the ground electrode. However, the AC whipping envelope

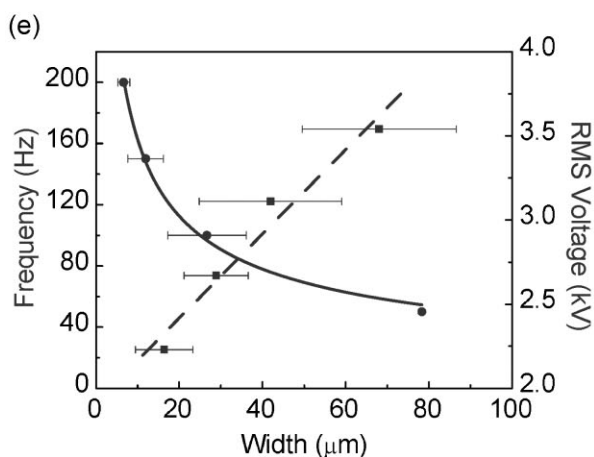
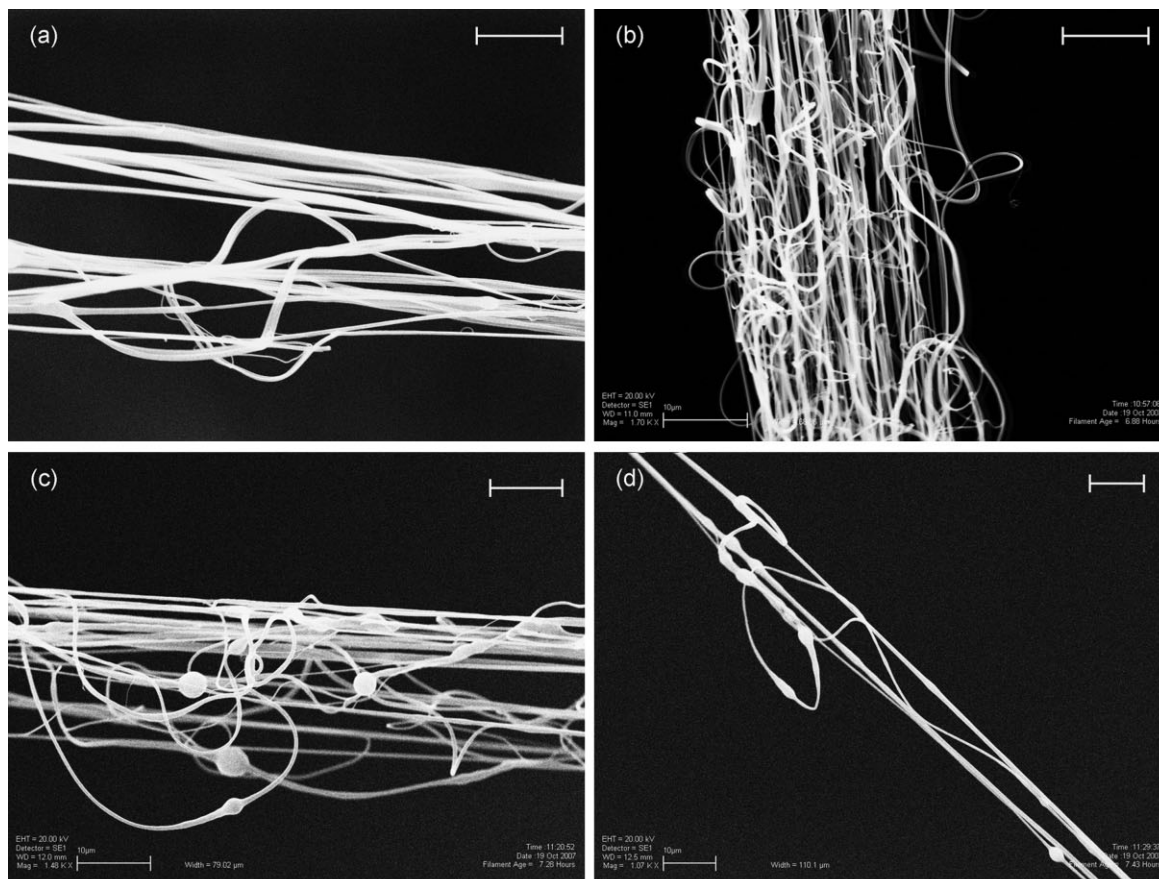


**Figure 3.** SEM images of threads consisting of multiple strands obtained at different voltages and frequencies, scale bar: 10  $\mu\text{m}$ . a) 2.23 kV, 50 Hz; b) 3.33 kV, 50 Hz; c) 3.33 kV, 100 Hz; d) 3.33 kV, 150 Hz. Number of strands increase with frequency and decrease with voltage. e) Variation of net thread width with frequency (purple) and voltage (blue). An inverse trend with frequency and a linear trend with voltage are clearly seen.

cannot be explained similarly, since it was independent of the ground electrode dimension and could be seen with both sharp and wide ground electrodes. In order to further comprehend this whipping pattern, collectors were placed in the whipping zone at different distances from the needle electrode to collect the fibers and find the characteristic length scale of the fiber spread, as shown in Figures 4e–g. We had placed a glass collector in between the live needle and the ground electrode. The distance between the needle and the ground electrode was fixed at 20 mm, and only the collector location was varied (5, 11, and 17 mm from the

needle). Hence, the variation in the magnitude of the electric field was negligible. It was found that this fiber spread length scale was decreasing with distance, which again pointed to a conical shape with its tip pointing downwards, as confirmed by Figure 4c. A similar trend was observed at higher applied frequencies, as shown in Figure 4d, verifying the presence of the inverted cone. Another key observation was the deposition pattern seen at different distances, showing that the fibers were forming a peripheral ring when the collector was close to the needle (Fig. 4e and f). Further away from the needle, as shown in Figure 4g, there

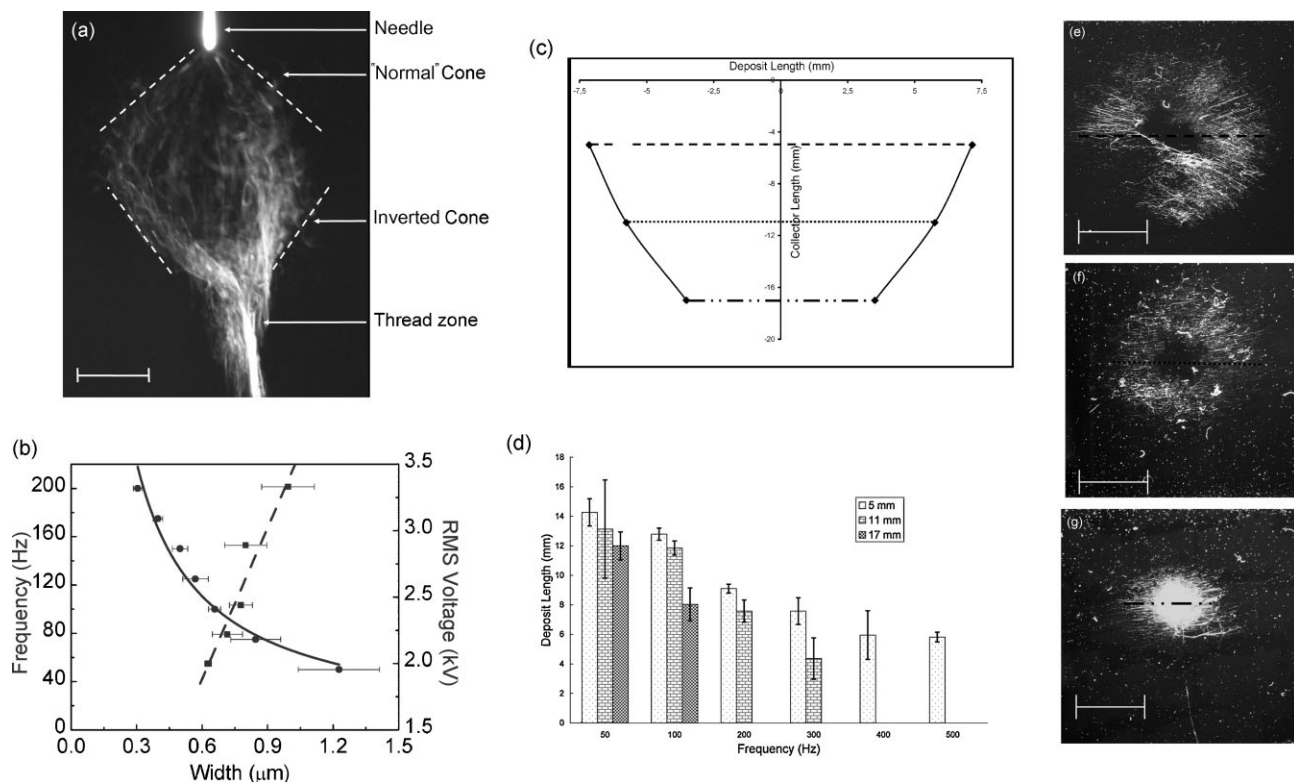


**Figure 4.** The whipping zone, scale bar: 5 mm. a) Long Exposure (0.02 s) image of the spinning process. The whipping envelope can be seen as a combination of a normal upright cone and an inverted cone. A distinct thread zone is seen below the apex of the inverted cone. b) Variation of the area of the whipping envelope with frequency (purple) and voltage (blue). The variation is linear with voltage and inverse with frequency. c) The length scale of the fiber deposit obtained on collectors plotted against the collector distance to the needle tip, confirming the presence of an inverted conical structure. The corresponding fiber deposits are shown in e–g. d) Fiber deposit length scales obtained at different distances at different frequencies. The length scales decrease with both frequency and collector distance. e) Fiber deposit on a collector placed 5 mm away from the needle tip. f) Fiber deposit on a collector placed 11 mm away from the needle tip. g) Fiber deposit on a collector placed 17 mm away from the needle tip obtained after collection for 2 s. The dashed lines in e–g, representing the length scale of the fiber deposit, are used in c.

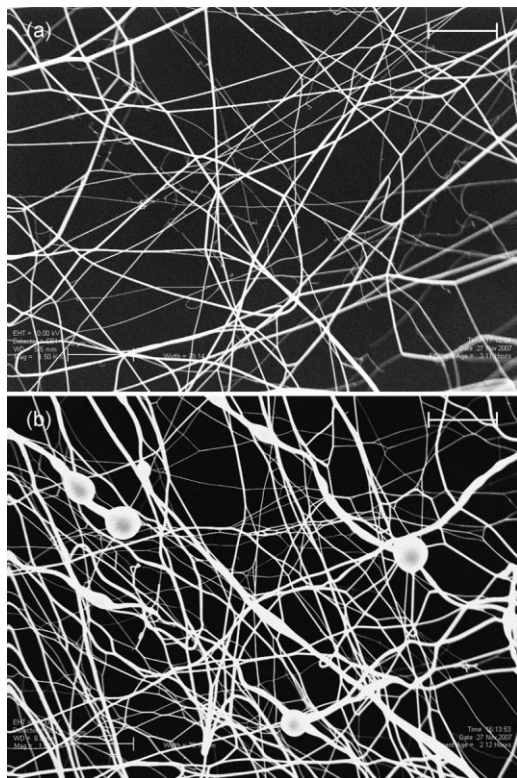
was a solid circle of deposits seen. Thus, we can get a clearer representation of the actual fiber path in the whipping cloud.

Figure 5 shows some SEM micrographs of these deposits observed within the whipping cloud, which were found to be similar to the mesh-like morphology under DC electrospinning. Consequently it is possible to produce fiber morphologies similar to DC electrospinning by placing the collectors within the whipping cloud. This similarity is expected since in DC spinning, the fibers are predominantly collected within the whipping zone. The effect of the applied frequency on the electrospun fiber morphology could also be seen. With an increase in frequency the fibers in the mesh network became thicker and bead formation on the fibers was more prevalent, which was similar to the effects seen with the thread morphology shown in Figure 3. We would like to re-emphasize that very different morphologies, threads, and mesh networks can be obtained via AC electrospinning by varying the collector location and the applied potential and frequency.

In order to understand these varied fiber morphologies, it was imperative that the liquid meniscus be examined critically, since our previous work with AC electrospinning had clearly indicated that the introduction of the frequency time scale and the periodic reversal of polarity caused significant changes in the liquid

meniscus, thus altering the spraying characteristics.<sup>[22,23]</sup> The meniscus observation was carried out with high-speed imaging because of the rapid dynamics of this process, in order to delineate the different effects present. We could distinguish three additional effects due to the use of an AC field. Firstly, the liquid jet was oscillating at the applied frequency, which was responsible for the absence of any significant linear portion in the jet. This is not surprising since the charge on the liquid jet was alternating with the applied frequency. Secondly, there could be multiple jets emerging out from the meniscus as depicted in Figure 6a, producing fibers every half cycle. This is an effect that we had previously seen in low frequency AC electrospinning and resonance<sup>[25]</sup> where multiple cones were formed, with drops being ejected out every half cycle.

However, the most dramatic effect that was seen near the meniscus was the production of branched fibers. There was a primary jet emerging from the meniscus and there were secondary jets emerging from the body of the main jet. To ensure that this was not an optical artifact induced due to the self-weaving, it was examined very carefully with high frame rates (5000 fps) and fast shutter speeds (0.02 ms), which confirmed the occurrence of this effect. As shown in Figure 6b, one can notice the emergence of fibers from the main jet, giving the appearance



**Figure 5.** SEM images of the mesh-like fibers obtained within the whipping zone at 3.3 kV at different frequencies, scale bars: 10  $\mu\text{m}$ . a) 50 Hz. b) 300 Hz. Increase in bead formation and thicker fibers are seen at higher frequencies.

of branches emerging from a main stem. This branching behavior had also been seen with DC electrospinning,<sup>[26]</sup> and has been modeled as surface undulations due to capillary and electrical stresses.<sup>[27]</sup> However, there were certain key differences between the DC and AC branching phenomenon. In DC spinning, there was generally a main jet with branches that were quite small compared to the main jet and the time scale for the branching event that was reported as approximately  $10 \text{ s}^{-1}$ . In contrast, the AC branches were quite long and individual branches could split further, as shown in Figure 6c. Moreover, branching took place every half cycle, and so the time scale was determined by the applied frequency. As shown in Figures 2 and 3, the threads that were observed in AC electrospinning were not just superimposed together, but formed a continuous network. This could be a direct manifestation of the branching phenomenon. We believe that the strong presence of branching is enhanced in AC electrospinning due to the use of a sine waveform. During one AC cycle there is a significant fraction of time when the Maxwell force on the fiber is very small due to the applied potential having a small value. This results in partial solidification of the fiber branches without significant extension, making it more favorable for fiber jets to take a side path.

An apparent result of the frequency timescale was the formation of fibers with both positive and negative segments because the fibers were being produced continuously while the polarity was switching every half cycle. This was clearly responsible for the high degree of aerial self-weaving that we

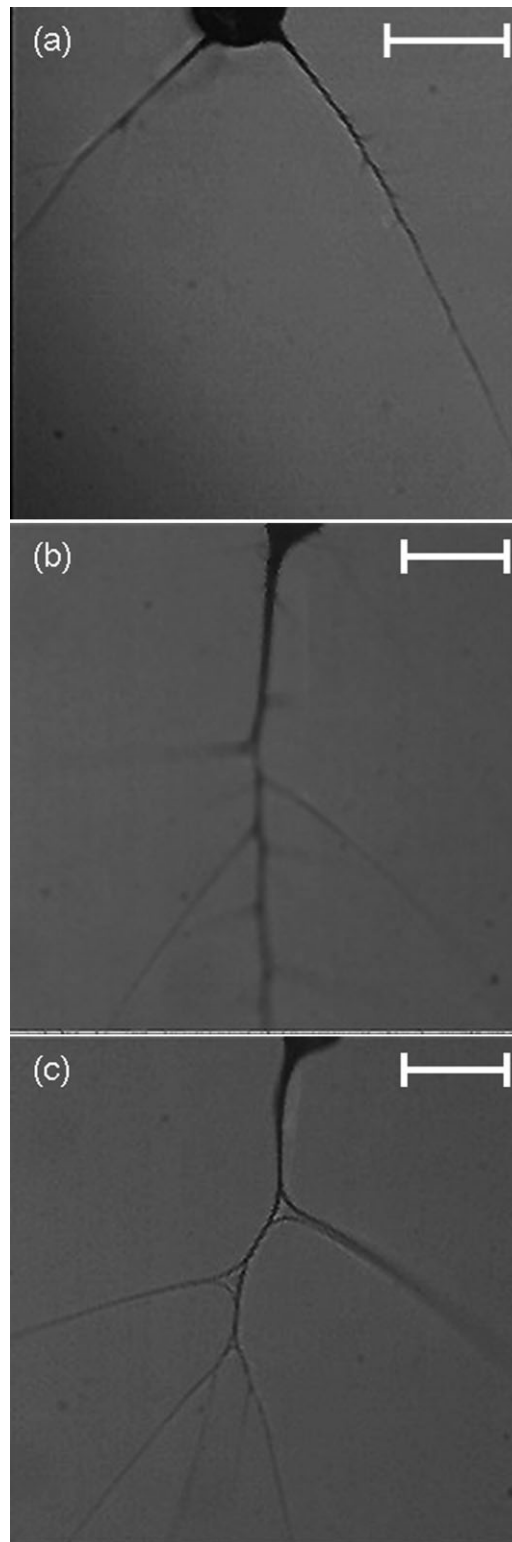


**Figure 6.** Images of the electrospinning jet emerging from the meniscus, scale bars: 300  $\mu\text{m}$ . a) Two jets emerging from the meniscus forming multiple fibers out of the same meniscus. b) A single jet branching out to form a vein-like structure in the fibers. c) Higher order branching of the fibers.

had observed, due to the fact that different segments of the fibers were experiencing an attractive and repulsive force at the same time. Additionally, the presence of both positive and negative elements in the fiber resulted in increased stabilization and alignment of the resultant fibers since charge repulsion effects were reduced as compared to DC electrospinning.

Another key feature was the contrasting effect of the applied potential and frequency on the variation of the net width of the thread as well as the whipping envelope area, as shown in Figures 3e and 4b. Both the whipping area and the net width were linearly proportional to the electric potential and inversely proportional to the frequency, confirming that frequency had an opposing effect to voltage. To explain this, we need to examine the effect of the applied field conditions on the whipping instability. It is known that the applied potential enhances the whipping instability, since whipping is an electric field driven instability. Consequently it can be inferred that the frequency proves to be detrimental to whipping. A simple explanation for this is the reduction of time available for whipping with the increase in frequency, since the force is in the same direction only for one half cycle, which becomes shorter as the frequency increases. As mentioned previously, it is the whipping instability that is responsible for the increase in jet path length by approximately three orders of magnitude, leading to the formation of nanofibers in electrospinning. Hence, increasing frequency leads to a smaller whipping cloud as well as lesser extension of fibers. This is consistent with our results where we noticed a lower density and increasing bead formation with the increase in frequency, irrespective of whether the fibers were collected in the whipping zone (Fig. 5) or in thread zone (Fig. 3). A similar explanation justifies the opposite effect seen with the applied potential.

To summarize, we believe that AC electrospinning is a very versatile addition to this field, and provides a simple and inexpensive tool to generate fiber threads with a predetermined morphology that can be easily assembled into regimented fabrics. It is also shown that very different morphologies from threads to mesh networks can be obtained via this method, by simply varying the collector location and the applied potential and frequency. The fiber threads and the mesh networks are strongly interconnected to each other, and as such should prove to be very useful for specific applications like fabric weaving and filtration, as well as for biomedical applications due to their inherent mechanical strength. The higher degree of fiber alignment in the threads is an additional advantage.

## Experimental

The High AC potential for these experiments was generated by using a waveform generator (Agilent-33220A) connected to an RF amplifier (Powertron) and a high voltage output transformer (Industrial test equipment) capable of generating up to 6 kV<sub>RMS</sub> for a frequency range between 30 Hz and 1 kHz. We used Poly(vinyl pyrrolidone) (12% w/w) as the model polymer, given its low chemical toxicity and ease of solubility in water and organic solvents. 1-Butanol was used as the solvent instead of the more commonly used ethanol to avoid needle clogging due to the higher vapor pressure of ethanol. The experiments were carried out by passing the polymer solution through a fine metallic needle (Hamilton 91033, id

100  $\mu\text{m}$ ) that was connected to the high voltage terminal of the transformer. A desired polymer flowrate, between 0.15 and 0.5 mL h<sup>-1</sup>, was achieved by connecting the needle to a syringe pump (Harvard apparatus). A ground electrode, which was a flat metal plate, was placed at specific distances between 2 and 4 cm away below the needle, and the circuit was completed by connecting the grounded terminal of the output transformer to the ground electrode. A collecting plate, either a glass cover-slip or a metallic wire mesh, was placed at varying locations between the electrodes. The process was visualized using either a high speed camera system (Olympus-ispeed) connected directly to a microscope objective or via still images taken from a digital camera (Canon).

## Acknowledgements

The authors wish to acknowledge Korey Chu for his assistance in the project. Supporting Information is available online from Wiley InterScience or from the authors.

Received: March 14, 2008

Revised: May 25, 2008

Published online: November 10, 2008

- [1] D. Li, Y. Xia, *Adv. Mater.* **2004**, *16*, 1151.
- [2] Z.-M. Huang, Y.-Z. Zhang, M. Kotaki, S. Ramakrishna, *Compos. Sci. Technol.* **2003**, *63*, 2223.
- [3] H. Jia, G. Zhu, B. Vugrinovich, W. Kataphinan, D. H. Reneker, P. Wang, *Biotechnol. Prog.* **2002**, *18*, 1027.
- [4] P. W. Gibson, H. L. Schreuder-Gibson, D. Rivin, *AIChE J.* **1999**, *45*, 190.
- [5] X. Wang, C. Drew, S.-H. Lee, K. J. Senecal, J. Kumar, L. A. Samuelson, *Nano Lett.* **2002**, *2*, 1273.
- [6] C. J. Buchko, L. C. Chen, Y. Shen, D. C. Martin, *Polymer* **1999**, *40*, 7397.
- [7] G. E. Wnek, M. E. Carr, D. G. Simpson, G. L. Bowlin, *Nano Lett.* **2003**, *3*, 213.
- [8] H. Yoshimoto, Y. M. Shin, H. Terai, J. P. Vacanti, *Biomaterials* **2003**, *24*, 2077.
- [9] S. Ramakrishna, K. Fujihara, W.-E. Teo, T.-C. Lim, Z. Ma, *An Introduction to Electrospinning and Nano-fibers*, World Scientific, Singapore **2005**.
- [10] G. Taylor, *Proc. R. Soc. London A* **1964**, *280*, 383.
- [11] A. L. Yarin, S. Koombhongse, D. H. Reneker, *J. Appl. Phys.* **2001**, *90*, 4836.
- [12] D. H. Reneker, A. L. Yarin, H. Fong, S. Koombhongse, *J. Appl. Phys.* **2000**, *87*, 4531.
- [13] Y. M. Shin, M. M. Hohman, M. P. Brenner, G. C. Rutledge, *Appl. Phys. Lett.* **2001**, *78*, 1149.
- [14] Y. M. Shin, M. M. Hohman, M. P. Brenner, G. C. Rutledge, *Polymer* **2001**, *42*, 09955.
- [15] M. M. Hohman, M. Shin, G. Rutledge, M. P. Brenner, *Phys. Fluids* **2001**, *13*, 2201.
- [16] D. Sun, C. Chang, S. Li, L. Lin, *Nano Lett.* **2006**, *6*, 839.
- [17] D. Li, G. Ouyang, J. T. McCann, Y. Xia, *Nano Lett.* **2005**, *5*, 913.
- [18] E. Zussman, A. Theron, A. L. Yarin, *Appl. Phys. Lett.* **2003**, *82*, 973.
- [19] R. Kessick, J. Fenn, G. Tepper, *Polymer* **2004**, *45*, 2981.
- [20] L. Y. Yeo, Z. Gagnon, H.-C. Chang, *Biomaterials* **2005**, *26*, 6122.
- [21] S. Sarkar, S. Deevi, G. Tepper, *Macromol. Rapid Commun.* **2007**, *28*, 1034.
- [22] S. Maheshwari, H.-C. Chang, *Appl. Phys. Lett.* **2006**, *89*, 234103.
- [23] S. Maheshwari, H.-C. Chang, *J. Appl. Phys.* **2007**, *102*, 034902.
- [24] A. Theron, E. Zussman, A. L. Yarin, *Nanotechnology* **2001**, *12*, 384.
- [25] P. Wang, S. Maheshwari, H. C. Chang, *Phys. Rev. Lett.* **2006**, *96*, 254502.
- [26] S. Koombhongse, W. Liu, D. H. Reneker, *J. Polym. Sci., Part B: Polym. Phys.* **2001**, *39*, 2598.
- [27] A. L. Yarin, W. Kataphinan, D. H. Reneker, *J. Appl. Phys.* **2005**, *98*, 064501.